AIP | Applied Physics Letters

Contact resistivities of metal-insulator-semiconductor contacts and metal-semiconductor contacts

Hao Yu, Marc Schaekers, Kathy Barla, Naoto Horiguchi, Nadine Collaert, Aaron Voon-Yew Thean, and Kristin De Meyer

Citation: Applied Physics Letters **108**, 171602 (2016); doi: 10.1063/1.4947580
View online: http://dx.doi.org/10.1063/1.4947580
View Table of Contents: http://scitation.aip.org/content/aip/journal/apl/108/17?ver=pdfcov
Published by the AIP Publishing

Contact resistivities of metal-insulator-semiconductor contacts and metal-semiconductor contacts

Hao Yu (于浩),[1,2] Marc Schaekers,[2] Kathy Barla,[2] Naoto Horiguchi,[2] Nadine Collaert,[2] Aaron Voon-Yew Thean,[2] and Kristin De Meyer[1,2]
[1]*ESAT Department, Katholieke Universiteit Leuven, Leuven B-3001, Belgium*
[2]*Imec, Kapeldreef 75, Leuven B-3001, Belgium*

(Received 17 November 2015; accepted 14 April 2016; published online 25 April 2016)

Applying simulations and experiments, this paper systematically compares contact resistivities (ρ_c) of metal-insulator-semiconductor (MIS) contacts and metal-semiconductor (MS) contacts with various semiconductor doping concentrations (N_d). Compared with the MS contacts, the MIS contacts with the low Schottky barrier height are more beneficial for ρ_c on semiconductors with low N_d, but this benefit diminishes gradually when N_d increases. With high N_d, we find that even an "ideal" MIS contact with optimized parameters cannot outperform the MS contact. As a result, the MIS contacts mainly apply to devices that use relatively low doped semiconductors, while we need to focus on the MS contacts to meet the sub-1×10^{-8} Ω cm^2 ρ_c requirement for future Complementary Metal-Oxide-Semiconductor (CMOS) technology. *Published by AIP Publishing.* [http://dx.doi.org/10.1063/1.4947580]

The strong surface Fermi-level pinning induces large Schottky barrier heights (ϕ_b) of metal-semiconductor (MS) contacts on n-Si, n-Ge, and several other semiconductors regardless of the metal work function.[1,2] By simply inserting an ultrathin dielectric layer—such as TiO_x,[3–8] AlO_x,[9–11] Si_3N_4,[9,12,13] MgO,[14,15] etc.[16–20]—between the metal and the semiconductor, ϕ_b can be efficiently lowered down to 0.2 eV or even further. Intuitively, we would expect that this type of metal-insulator-semiconductor (MIS) contacts with such a low ϕ_b easily outperforms the MS contacts in terms of contact resistivities (ρ_c). This expectation has also been widely demonstrated on low and moderately doped substrates.[3–27] However, on highly doped semiconductors, the lowest reported ρ_c of MIS have been merely $\sim1\times10^{-8}$ $\Omega\cdot$cm^2 for n-Si[7,28] and $\sim1\times10^{-7}$ $\Omega\cdot$cm^2 for n-Ge,[20,23] while those of MS contacts have reached $\sim2\times10^{-9}$ $\Omega\cdot$cm^2 for n-Si[8,29] and $\sim2\times10^{-8}$ $\Omega\cdot$cm^2 for n-Ge.[30,31] It seems that MIS mainly benefits semiconductors with relatively low doping concentrations (N_d), but they lose the advantages with high N_d.[32,33] In the previous studies, MIS has rarely been compared systematically with MS at a large range of semiconductor doping levels; especially, the experimental study is lacked. To fill this gap, we perform both experimental and simulation comparisons of MIS and MS with various N_d. Based on that, we will discuss why MIS loses the ρ_c advantage over MS on highly doped semiconductors.

For a quantitative analysis, a ρ_c calculation model is developed, which allows us to compare the MIS and MS contacts in depth. This model is based on the prior knowledge of the MS contacts: applying Wentzel–Kramers–Brillouin (WKB) approximations, Stratton develops an expression for the carrier tunneling behavior through an arbitrary potential barrier;[34] based on that, Padovani and Stratton built the formula of the current voltage (IV) behavior through Schottky barriers,[35] Yu deduced the ρ_c formula for the MS contacts with intermediate and high N_d,[36] and Ng applied an effective tunneling mass correction for the ρ_c calculation.[37]

Similar to Yu,[36] we focus on semiconductors with N_d of 10^{18}–10^{21} cm^{-3}, whose carrier conduction through the contact is based on thermionic-field emission (TFE) or field emission (FE).[35] Carrier tunneling is the underlying mechanism behind TFE and FE; hence, the carrier tunneling probability, P, is the key variable in the ρ_c calculation. Assuming parabolic energy-momentum relations in the semiconductor, the WKB approximations simplify the P calculation to[34]

$$\ln P(E_x) = -\alpha\int_0^w [\phi(x)-E_x]^{1/2}dx, \tag{1a}$$

$$E_x = \frac{p_x^2}{2m^*}, \tag{1b}$$

$$\alpha = \frac{2(2m^*)^{1/2}}{\hbar}, \tag{1c}$$

where ϕ(x) is the potential energy equation that describes the shape of the barrier, w is the barrier width, E_x and p_x are the carrier energy and the carrier momentum perpendicular to the barrier, m* is the effective carrier mass, and $\hbar$ is the reduced Planck's constant. Since (1a) cannot be solved analytically for an arbitrary ϕ(x) equation, Stratton applies the Taylor expansion to it[34]

$$\ln P(E_x) = -(b + c\epsilon_x + f\epsilon_x^2\ldots), \tag{2a}$$

$$\epsilon_x = E_r - E_x, \tag{2b}$$

$$b = \alpha\int_0^w [\phi(x)-E_r]^{1/2}dx, \tag{2c}$$

$$c = \frac{1}{2}\alpha\int_0^w [\phi(x)-E_r]^{-1/2}dx, \tag{2d}$$

$$f = -\frac{1}{8}\alpha\int_0^w [\phi(x)-E_r]^{-3/2}dx, \tag{2e}$$

where ϵ_x is an intermediate variable that transforms (1a) into an equation with respect to the reference energy level, E_r. In other words, (2a) is a Taylor series of (1a) at the energy level E_r. The quadratic and higher order terms in (2a) can be neglected if the boundary condition $1 - ckT > kT(2f)^{1/2}$ is met.[35] In principle, E_r should be selected close to the level where there is a maximum carrier tunneling.[34]

Applying Taylor series for the ln $P(E_x)$ expression is remarkable: it not only enables a numerical calculation of tunneling probability for an arbitrary barrier but it also simplifies the expression of the IV behavior. By placing the Schottky barrier equation, $\phi_s(x)$, into (2a), the IV behavior and ρ_c for the MS contacts are successfully derived.[35,36] Interestingly, we find that the influence of an insulator in MIS can also be incorporated into (1a) and (2a) in a simple way: the total tunneling probability $P(E_x)$ through MIS can be calculated by

$$P(E_x) = P_s(E_x) \times P_i(E_x), \tag{3}$$

i.e.,

$$\ln P(E_x) = \ln P_s(E_x) + \ln P_i(E_x), \tag{4}$$

where $P_s(E_x)$ and $P_i(E_x)$ are the tunneling probabilities through the semiconductor barrier and insulator barrier, respectively. Similar to (2a), we carry out the Taylor expansion for ln $P_s(E_x)$ and ln $P_i(E_x)$

$$\begin{aligned}\ln P_s(E_x) &= -\alpha \int_0^w [\phi_s(x) - E_x]^{1/2} dx \\ &= -(b_s + c_s\epsilon_x + f_s\epsilon_x^2 \ldots),\end{aligned} \tag{5}$$

$$\ln P_i(E_x) = -\alpha \int_0^t [\phi_i(x) - E_x]^{1/2} dx = -(b_i + c_i\epsilon_x + f_i\epsilon_x^2 \ldots), \tag{6}$$

where $\phi_i(x)$ are the potential barrier equations for the insulator, and t is the insulator thickness. After calculating the Taylor series for ln $P_s(E_x)$ and ln $P_i(E_x)$ with (5) and (6), ln P (E_x), the sum in (4), is easily calculated. Eventually, the ρ_c of the MIS contacts is derived.[36]

Following the aforementioned methodology, three steps are taken for the MIS ρ_c calculations: (a) build the barrier equations $\phi_s(x)$ and $\phi_i(x)$; (b) derive the Taylor series for ln $P_s(E_x)$ and ln $P_i(E_x)$; and (c) calculate the ρ_c of the MIS. As a case study, the MIS contacts on n-Si(100) are taken, and a schematic energy band diagram is shown in Fig. 1(a).

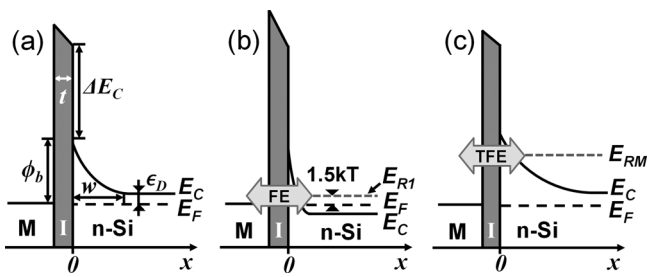

FIG. 1. (a) Schematic band diagram of MIS on n-Si(100) including key parameters. With a constant ϕ_b, MIS band diagram with (b) high N_d and (c) intermediate N_d is compared.

Similar to previous studies,[35,36,38] we apply the 1D Poisson equation and the depletion approximation for $\phi_s(x)$

$$\phi_s(x) = \frac{qN_d}{2\varepsilon_{rs}\varepsilon_0}(w - x)^2, \tag{7a}$$

where

$$w = \sqrt{\frac{2\varepsilon_{rs}\varepsilon_0(\phi_b - \epsilon_D)}{qN_d}}, \tag{7b}$$

$$\epsilon_D = E_C - E_F. \tag{7c}$$

N_d is the active donor concentration, w is the depletion width, ε_{rs} is the relative dielectric constant of the semiconductor, ε_0 is the vacuum electric permittivity, and E_C and E_F are the conduction band minimum and the Fermi energy level, respectively. The energy difference ϵ_D is a function of N_d, which is solved using the Fermi-Dirac distribution and dopant ionization functions.[39,40]

To build $\phi_i(x)$, knowledge of the electric field in the insulator (F_i) is required. As a general discussion, we neglect the interfacial charges and the fixed charges in the insulator for simplicity. With continuity of the electric displacement, the electric field at the semiconductor surface (F_{ss}) and F_i has the relation

$$\varepsilon_{rs}\varepsilon_0 F_{ss} = \varepsilon_{ri}\varepsilon_0 F_i\,, \tag{8}$$

where ε_{ri} is the relative dielectric constant of the insulator. With the depletion approximation,

$$F_{ss} = \frac{qN_D w}{\varepsilon_{rs}\varepsilon_0}. \tag{9}$$

With (8),

$$F_i = \frac{qN_D w}{\varepsilon_{ri}\varepsilon_0}. \tag{10}$$

Then,

$$\phi_i(x) = q\phi_b + \Delta E_c - \epsilon_D - \frac{q^2 N_D w}{\varepsilon_s\varepsilon_0}x\,. \tag{11}$$

After building $\phi_s(x)$ and $\phi_i(x)$, we only need to define E_R before carrying out the Taylor expansions. Since E_R has to be defined close to the level that has a maximum carrier tunneling flux, different criteria have to be applied for FE and TFE, respectively. FE dominates when the semiconductor barrier is thin (Fig. 1(b)). In the previous works,[34–36] E_F is selected as E_R for FE, because these studies cover the cryogenic operations: at cryogenic temperatures, the electrons close to E_F have the highest kinetic energy and they also see the thinnest tunneling barrier. But at room temperature, E_F is unfavorable as E_R, which makes those ρ_c calculations[35,36] invalid for low-ϕ_b contacts. Since this paper mainly focuses on ρ_c at room temperature, considering the product of $D(E_x)$ and $P(E_x)$, we define $E_{R1} = E_F + 1.5kT$ (k is the Boltzmann constant and T is the temperature) for FE, as shown in Fig. 1(b). This selection of E_{R1} allows a more accurate and flexible ρ_c calculation at room temperature, which also applies to low-ϕ_b contacts. Since at room temperature, FE is mainly related with degenerate

semiconductors, whose E_{R1} is located in the conduction band of the semiconductor, the range of the integral in (2a) needs to be modified from $0 \sim w$ to $0 \sim w_1$. w_1 is the position near the semiconductor surface, where $E_C(w_f) = E_{R1}$. TFE dominates when the semiconductor barrier is relatively thick (Fig. 1(c)). In this case, most of the carrier tunneling occurs close to the top of $\phi_s(x)$ where the barrier is thin enough for carriers to tunnel through. For TFE, same as Stratton[38] and Padovani,[35] E_{RM} is numerically calculated following the criterion $c_m kT = 1$ and (2d), where c_m is the coefficient of the quadratic term in the Taylor series of ln $P(E_x)$.

Eventually, for both FE and TFE, the Taylor expansions of ln $P_i(E_x)$ and ln $P_s(E_x)$ are carried out following (5) and (6), the Taylor series of ln $P(E_x)$ is easily calculated with (4), and the ρ_c of the MIS contacts is derived. For FE,[36]

$$\rho_c = \left[\frac{A\pi qT}{k\sin(\pi c_1 kT)}\exp(-b_1) - \frac{Ac_1 q}{(c_1 k)^2}\exp(-b_1 + c_1\epsilon_D)\right]^{-1}, \tag{12a}$$

where

$$A = \frac{m_e^* qk^2}{2\pi^2\hbar^3} \tag{12b}$$

is the Richardson constant, m_e^* is the electron effective mass in the conduction band of the semiconductor, and b_1, c_1, and f_1 are the polynomial coefficients in the Taylor series of ln $P(E_x)$ for FE. The above equation is valid when $(\sqrt{2f_1} + c_1)kT < 1$ and $\epsilon_D < 0$.

For TFE,[38]

$$\rho_c = \left[\frac{Aq}{2k^2}\left[\sqrt{\frac{\pi}{f_m}} + 2(E_{RM} - E_C)\right] \times \exp\left[-b_m - \frac{\epsilon_D + (E_{RM} - E_C)}{kT}\right]\right]^{-1}, \tag{13}$$

where b_m and f_m are the polynomial coefficients in the Taylor series of ln $P(E_x)$ for TFE. The above equation is valid when $\epsilon_D > 0$ and $E_{RM} - E_C > 0$.

After the model construction, we compare the MS and MIS contacts based on both experiments and simulations. In the experiment, P ion implanted (P I/I) Si substrates with N_d of 2.0×10^{18}, 1.5×10^{19}, 7.0×10^{19}, and $2.8 \times 10^{20}\,cm^{-3}$ were prepared on 300 mm Si wafers. P *in situ* doped epitaxial Si substrates (Si:P)[41] with high N_d of 3.0×10^{20}, 8.0×10^{20}, and $9.0 \times 10^{20}\,cm^{-3}$ were also prepared. Circular transmission line models (CTLM) and multiring CTLM (MR-CTLM) were fabricated for ρ_c extraction: CTLM applies to a large range of ρ_c between 10^{-8} and $10^{-1}\,\Omega\cdot cm^2$,[42] while MR-CTLM is used to accurately determine ultralow ρ_c from 10^{-9} to $10^{-7}\,\Omega\cdot cm^2$.[43] The detailed fabrication process and ρ_c extraction procedures for CTLM and MR-CTLM can be found in our previous reports.[42,43] On the MS wafers, 5nm Ti and 10 nm TiN were deposited on Si in sequence as contact metal using low-bias physical vapor deposition, while on the MIS wafers, the Ti/TiN deposition was preceded by ~1.4 nm TiO_2 atomic layer deposition (ALD). A low-thermal budget post-metal process was carried out to protect the Ti/TiO_2 interface in the MIS contacts.[8]

Interesting contrasts are observed in Fig. 2: for relatively low doped n-Si with N_d of 2.0×10^{18} and $1.5 \times 10^{19}\,cm^{-3}$, the ρ_c of Ti/TiO_2/n-Si is lower than that of Ti/n-Si; however, when N_d is higher than $4 \times 10^{19}\,cm^{-3}$, the Ti/n-Si outperforms the Ti/TiO_2/n-Si. The experimental data are then fitted using the ρ_c model. Good agreements are achieved between the extracted ϕ_b from the fitting (Fig. 2) and ϕ_b from our previous Schottky barrier study[8] where ϕ_b of Ti/n-Si is 0.46–0.48 eV, while ϕ_b of Ti/(~0.8 nm)TiO_2/n-Si is ~0.14 eV. Combined with the schematic of Figs. 1(b) and 1(c), the crossover of the ρ_c-N_d curves of Ti/n-Si and Ti/TiO_2/n-Si in Fig. 2 can be understood qualitatively: on lowly doped Si ($N_d < 4 \times 10^{19}\,cm^{-3}$), the semiconductor barrier is thick and dominant, so that the thermionic-field emission (TFE) through Ti/TiO_2/n-Si with a low ϕ_b is much easier than that through Ti/n-Si; however, on highly doped Si, the semiconductor barrier becomes thin and minor compared with the TiO_2 barrier so that the field emission (FE) in Ti/n-Si is much easier than Ti/TiO_2/n-Si in spite of a relatively high ϕ_b of ~0.5 eV.

In the ρ_c-N_d curve fitting for Ti/TiO_2/n-Si in Fig. 2, the TiO_2 thickness (t) is determined with XTEM, and the effective electron tunneling mass (m_{ti}^*) and the dielectric constant (ε_{ri}) of TiO_2 are taken from the literature.[44] The Ti/Si conduction band offset ΔE_C of ~0.55 eV and ϕ_b of ~0.1 eV are directly extracted from the fitting. The ΔE_C of ~0.55 eV is close to the values of 0.6–0.8 eV determined from the internal electron photoemission (IPE) spectroscopy[45] and is different from the zero ΔE_C in the previous simulation reports.[46] This is because the crystalline TiO_2 parameters are used in the simulation[46] but an amorphous ALD TiO_2 is applied in the IPE experiment[45] and in this work. The amorphous TiO_2 has a ~1 eV larger band gap and a much higher ΔE_C with respect to Si than the crystalline TiO_2.[45,47] In the previous MIS simulation studies, Roy *et al.*[44] and Agrawal *et al.*[48] concluded that TiO_2 is an optimal candidate for the MIS contacts on n-Ge or n-Si. These conclusions are actually based on the zero ΔE_C assumption of TiO_2, while the realistic ΔE_C of ~0.6 eV clearly makes amorphous TiO_2 a less ideal candidate for MIS. Unfortunately, the as deposited ~1 nm

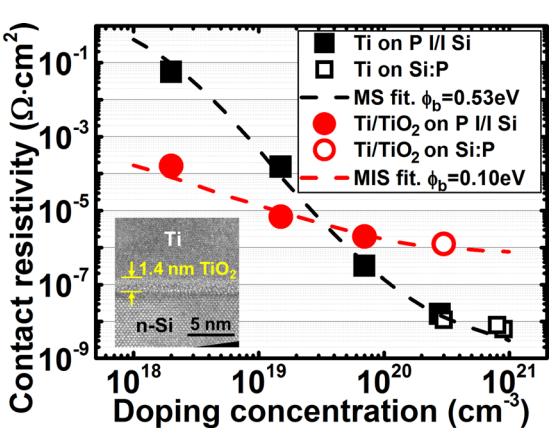

FIG. 2. Experimental ρ_c-N_d data of Ti/n-Si MS and Ti/TiO_2/n-Si MIS contacts and curve fitting. Each symbol is an averaged ρ_c measured with four sets of CTLM or MR-CTLM. Dashed lines are fitting curves. The fitting parameter for Ti/n-Si is $\phi_b = 0.53$ eV; and those for Ti/TiO_2/n-Si are $\phi_b = 0.1$ eV, t = 1.4 nm, $\Delta E_C = 0.55$ eV, $m_{ti}^* = 0.3\ m_0$, and $\varepsilon_{ri} = 80$. The inset is an XTEM image of Ti/TiO_2/n-Si.

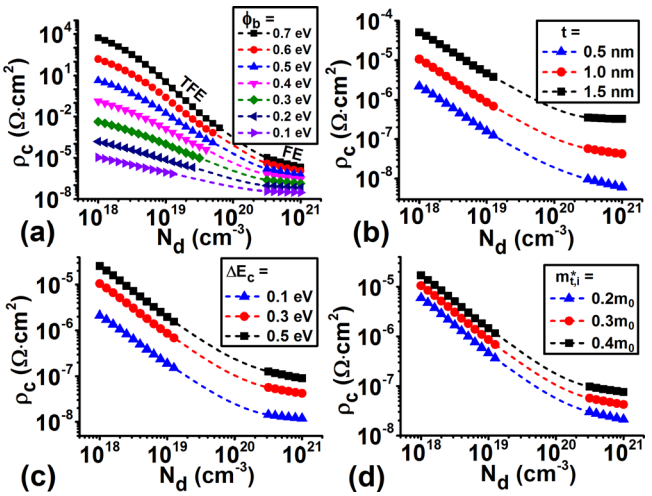

FIG. 3. Simulation of ρ_c-N_d curves of MIS contacts using a set of default parameters: $\phi_b = 0.1$ eV, t = 1 nm, $\Delta E_C = 0.3$ eV, $m^*_{ti} = 0.3m_0$, and $\varepsilon_{ti} = 80$. Then, based on default settings, (a) ϕ_b, (b) t, (c) ΔE_C, and (d) m^*_{ti} are varied individually to illustrate their impacts on ρ_c.

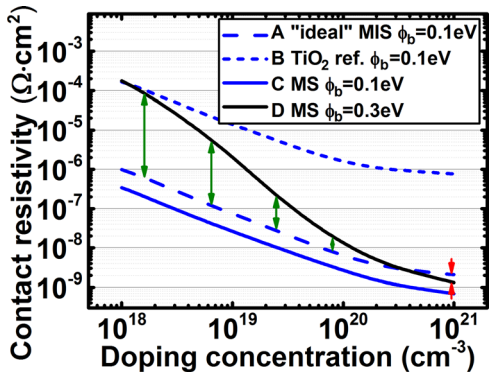

FIG. 4. Comparison of ρ_c-N_d curves of MIS and MS on n-Si(100) based on simulations. The curves are named with A–D for simplicity. A is hypothetically assigned with superior parameters: $\phi_b = 0.1$ eV, t = 0.5 nm, $\Delta E_C = 0.1$ eV, and $m^*_{ti} = 0.2m_0$. B is the Ti/TiO_2/n-Si MIS fitting curve in Fig. 2 with parameters of $\phi_b = 0.1$ eV, t = 1.4 nm, $\Delta E_C = 0.55$ eV, and $m^*_{ti} = 0.3\ m_0$. C and D are MS references. The green and red arrows denote the ρ_c differences between A and D.

ALD TiO_2 is always at an amorphous state, while we found that the thermal treatment at even 750 °C can hardly crystallize this ultrathin TiO_2.

After the case study of the Ti/n-Si and Ti/TiO_2/n-Si contacts, it is interesting to generally compare the lower ρ_c limits between the MS and MIS contacts. For MS contacts, N_d and ϕ_b are dominating factors. As shown in Fig. 2, ultrahigh N_d approaching 1×10^{21} cm^{-3} is achievable for n-Si.[41] With rare earth silicides as contact metal, low $\phi_b \sim 0.3$ eV have been demonstrated for MS contacts.[49,50] For MIS contacts, as shown in Fig. 3, their ρ_c correlates strongly with ϕ_b, t, m^*_{ti}, and ΔE_C. For instance, in Fig. 2, the relatively high t, m^*_{ti}, and ΔE_C of the Ti/TiO_2/n-Si contacts lead to a high ρ_c above 1×10^{-6} Ω·cm^2 even with N_d. In Fig. 4, we hypothetically model an "ideal" MIS with optimized parameters on n-Si (A) and compare it with the TiO_2 MIS reference in Fig. 2 (B) and the MS references with ϕ_b of 0.1 eV (C) and 0.3 eV (D). (Because of the Fermi-level pinning at the Si surface, C does not exist in reality.)

In Fig. 4, we see that the ρ_c-N_d curves of A, B, and C are almost in parallel, which means that the insulator in the MIS contacts augments ρ_c by a similar degree for any N_d. The advantage of the MIS contacts is most pronounced at relatively low doping levels, but it diminishes gradually with increasing N_d—at ultrahigh doping levels, even the "ideal" MIS, A, cannot outperform its MS counterpart, D. Moreover, the existence of such an "ideal" MIS as A is suspicious: for instance, insulators with m^*_{ti} as low as 0.2 m_0 are uncommon;[46,50] insulators that have low ΔE_C with semiconductors are rare;[44,46,50] moreover, there is usually a minimal insulator thickness of >1 nm required for an MIS to lower ϕ_b to 0.1 eV.[5,7,9,13] In conclusion, the MIS contacts are more appealing to the applications that use relatively low doped semiconductors, such as compound semiconductor devices and Si solar cells, while the MS contacts will still be the major force to push ρ_c down below 1×10^{-8} Ω·cm^2 to meet the Complementary Metal-Oxide-Semiconductor (CMOS) requirement for the 10 nm technology node and beyond.[51]

In summary, this paper systematically compares the contact resistivity of the MIS and MS contacts. A model is built for the quantitative ρ_c study and is verified by experiments. We find that the MIS contacts are more preferable on relatively low doped semiconductors due to their efficient Schottky barrier height modulation. However, on highly doped semiconductors, whose contact resistivity is much less sensitive to Schottky barrier height, the MS contacts are more desirable because of their less carrier tunneling difficulty.

[1]A. Dimoulas, P. Tsipas, A. Sotiropoulos, and E. K. Evangelou, Appl. Phys. Lett. **89**, 252110 (2006).
[2]T. Nishimura, K. Kita, and A. Toriumi, Appl. Phys. Lett. **91**, 123123 (2007).
[3]Z. Yuan, A. Nainani, Y. Sun, J. Y. J. Lin, P. Pianetta, and K. C. Saraswat, Appl. Phys. Lett. **98**, 172106 (2011).
[4]J. Hu, K. C. Saraswat, and H. S. Philip Wong, Appl. Phys. Lett. **99**, 092107 (2011).
[5]J. Y. J. Lin, A. M. Roy, A. Nainani, Y. Sun, and K. C. Saraswat, Appl. Phys. Lett. **98**, 092113 (2011).
[6]B.-Y. Tsui and M.-H. Kao, Appl. Phys. Lett. **103**, 032104 (2013).
[7]A. Agrawal, J. Lin, M. Barth, R. White, B. Zheng, S. Chopra, S. Gupta, K. Wang, J. Gelatos, S. E. Mohney, and S. Datta, Appl. Phys. Lett. **104**, 112101 (2014).
[8]H. Yu, M. Schaekers, E. Rosseel, A. Peter, J.-G. Lee, W.-B. Song, S. Demuynck, T. Chiarella, L.-Å. Ragnarsson, S. Kubicek, J. Everaert, N. Horiguchi, K. Barla, D. Kim, N. Collaert, A. V.-Y. Thean, and K. De Meyer, in *Technical Digest 2015—International Electron Devices Meeting (IEDM 2015)*, (2015), p. 592.
[9]T. Nishimura, K. Kita, and A. Toriumi, Appl. Phys. Express **1**, 051406 (2008).
[10]Y. Zhou, M. Ogawa, X. Han, and K. L. Wang, Appl. Phys. Lett. **93**, 202105 (2008).
[11]J. Hu, K. C. Saraswat, and H.-S. P. Wong, J. Appl. Phys. **107**, 063712 (2010).
[12]D. Connelly, C. Faulkner, P. A. Clifton, and D. E. Grupp, Appl. Phys. Lett. **88**, 012105 (2006).
[13]M. Kobayashi, A. Kinoshita, K. Saraswat, H.-S. P. Wong, and Y. Nishi, J. Appl. Phys. **105**, 023702 (2009).
[14]Y. Zhou, W. Han, Y. Wang, F. Xiu, J. Zou, R. K. Kawakami, and K. L. Wang, Appl. Phys. Lett. **96**, 102103 (2010).
[15]D. Lee, S. Raghunathan, R. J. Wilson, D. E. Nikonov, K. Saraswat, and S. X. Wang, Appl. Phys. Lett. **96**, 052514 (2010).
[16]R. R. Lieten, V. V. Afanas'ev, N. H. Thoan, S. Degroote, W. Walukiewicz, and G. Borghs, J. Electrochem. Soc. **158**, H358 (2011).
[17]Y.-L. Jiang, Q. Xie, X.-P. Qu, G.-P. Ru, D. W. Zhang, D. Deduytsche, and C. Detavernier, Electrochem. Solid-State Lett. **14**, H487 (2011).

[18]S. Zheng, W. Yang, Q. Q. Sun, L. Chen, P. Zhou, P. F. Wang, D. Wei Zhang, and F. Xiao, Appl. Phys. Lett. **103**, 261602 (2013).
[19]J. Hu, A. Nainani, Y. Sun, K. C. Saraswat, and H. S. Philip Wong, Appl. Phys. Lett. **99**, 252104 (2011).
[20]P. Paramahans Manik, R. Kesh Mishra, V. Pavan Kishore, P. Ray, A. Nainani, Y. C. Huang, M. C. Abraham, U. Ganguly, and S. Lodha, Appl. Phys. Lett. **101**, 182105 (2012).
[21]J. Y. Jason Lin, A. M. Roy, and K. C. Saraswat, IEEE Electron Device Lett. **33**, 1541 (2012).
[22]M. H. Liao and L. C. Chang, Appl. Phys. Lett. **103**, 072102 (2013).
[23]P. P. Manik and S. Lodha, Appl. Phys. Express **8**, 051302 (2015).
[24]K. Majumdar, R. Clark, T. Ngai, K. Tapily, S. Consiglio, E. Bersch, K. Matthews, E. Stinzianni, Y. Trickett, G. Nakamura, C. Wajda, G. Leusink, H. Chong, V. Kaushik, J. Woicik, C. Hobbs, and P. Kirsch, in *2014 Symposium on VLSI Technology* (2014), p. 218.
[25]G. Kim, J. Kim, S. Kim, J. Jo, C. Shin, J. Park, K. C. Saraswat, and H. Yu, IEEE Electron Device Lett. **35**, 1076 (2014).
[26]D. R. Gajula, P. Baine, M. Modreanu, P. K. Hurley, B. M. Armstrong, and D. W. McNeill, Appl. Phys. Lett. **104**, 012102 (2014).
[27]P. J. King, E. Arac, S. Ganti, K. S. K. Kwa, N. Ponon, and A. G. O'Neill, Appl. Phys. Lett. **105**, 052101 (2014).
[28]K. Ang, K. Majumdar, K. Matthews, C. D. Young, C. Kenney, C. Hobbs, P. D. Kirsch, and R. Jammy, in *Technical Digest 2012—International Electron Devices Meeting (IEDM 2012)*, (2012), p. 439.
[29]C. Ni, X. Li, S. Sharma, K. V. Rao, M. Jin, C. Lazik, V. Banthia, B. Colombeau, N. Variam, A. Mayur, H. Chung, R. Hung, and A. Brand, in *2015 Symposium on VLSI Technology* (2015), p. T118.
[30]S. Huang, F. Lu, W. Huang, C. Huang, and C. W. Liu, IEEE Electron Device Lett. **36**, 1114 (2015).
[31]H. Miyoshi, T. Ueno, K. Akiyama, Y. Hirota, and T. Kaitsuka, in *2014 Symposium on VLSI Technology* (2014), p. 146.
[32]S. Gupta, P. P. Manik, R. Kesh Mishra, A. Nainani, M. C. Abraham, and S. Lodha, J. Appl. Phys. **113**, 234505 (2013).
[33]J. Kim, P. J. Oldiges, H. Li, H. Niimi, M. Raymond, and P. Zeitzoff, in *Proceedings of the 2015 International Conference on Simulation for Semiconductor Processes Devices* (2015), p. 234.
[34]R. Stratton, J. Phys. Chem. Solids **23**, 1177 (1962).
[35]F. A. Padovani and R. Stratton, Solid State Electron. **9**, 695 (1966).
[36]A. Y. C. Yu, Solid State Electron. **13**, 239 (1970).
[37]K. K. Ng and R. Liu, IEEE Trans. Electron Devices **37**, 1535 (1990).
[38]R. Stratton, Phys. Rev. **125**, 67 (1962).
[39]S. M. Sze and K. K. Ng, *Physics of Semicondcutor Devices*, 3rd ed. (John Wiley & Sons, New York, 2007), p. 17.
[40]N. G. Nilsson, Appl. Phys. Lett. **33**, 653 (1978).
[41]E. Rosseel, H. B. Profijt, A. Y. Hikavyy, J. Tolle, S. Kubicek, G. Mannaert, C. L'abbe, K. Wostyn, N. Horiguchi, T. Clarysse, B. Parmentier, S. Dhayalan, H. Bender, J. W. Maes, S. Mehta, and R. Loo, ECS Trans. **64**, 977 (2014).
[42]H. Yu, M. Schaekers, T. Schram, N. Collaert, K. De Meyer, N. Horiguchi, A. Thean, and K. Barla, IEEE Electron Device Lett. **35**, 957 (2014).
[43]H. Yu, M. Schaekers, T. Schram, E. Rosseel, K. Martens, S. Demuynck, N. Horiguchi, K. Barla, N. Collaert, K. De Meyer, and A. Thean, IEEE Electron Device Lett. **36**, 600 (2015).
[44]A. M. Roy, J. Y. J. Lin, and K. C. Saraswat, IEEE Electron Device Lett. **31**, 1077 (2010).
[45]V. V. Afanas'ev, A. Stesmans, F. Chen, M. Li, and S. A. Campbell, J. Appl. Phys. **95**, 7936 (2004).
[46]J. Robertson, J. Vac. Sci. Technol. B **18**, 1785 (2000).
[47]V. V. Afanas'ev and A. Stesmans, J. Appl. Phys. **102**, 081301 (2007).
[48]A. Agrawal, N. Shukla, K. Ahmed, and S. Datta, Appl. Phys. Lett. **101**, 042108 (2012).
[49]K. N. Tu, R. D. Thompson, and B. Y. Tsaur, Appl. Phys. Lett. **38**, 626 (1981).
[50]N. Reckinger, X. Tang, V. Bayot, D. A. Yarekha, E. Dubois, S. Godey, X. Wallart, G. Larrieu, A. Łaszcz, J. Ratajczak, P. J. Jacques, and J.-P. Raskin, J. Appl. Phys. **104**, 103523 (2008).
[51]See http://www.itrs.net for "The International Technology Roadmap for Semiconductors (ITRS), 2013."